





THS

## 1 2556 681862841

### LIBRARY Michigan State University

This is to certify that the thesis entitled

## IDENTIFICATION OF THE TOTAL PERIPHERAL RESISTANCE BAROREFLEX

presented by

YING LI

has been accepted towards fulfillment of the requirements for the

Master of d

degree in

Department of Electrical Engineering

Major Professor's Signature

**Date** 

MSU is an Affirmative Action/Equal Opportunity Institution

PLACE IN RETURN BOX to remove this checkout from your record.

TO AVOID FINES return on or before date due.

MAY BE RECALLED with earlier due date if requested.

DATE DUE	DATE DUE
	DATE DUE

2/05 c:/CIRC/DateDue.indd-p.15

## IDENTIFICATION OF THE TOTAL PERIPHERAL RESISTANCE BAROREFLEX

 $\mathbf{B}\mathbf{y}$ 

Ying Li

#### **A THESIS**

Submitted to
Michigan State University
in partial fulfillment of the requirements
for the degree of

**MASTER OF SCIENCE** 

**Department of Electrical Engineering** 

2005

## **ABSTRACT**

#### Identification of the Total Peripheral Resistance Baroreflex

By

#### Ying Li

Feedback control of total peripheral resistance (TPR) by the arterial and cardiopulmonary baroreflex systems is a well-known mechanism for short-term blood pressure regulation. Conventional methods for measuring this TPR baroreflex mechanism aim to quantify only the static gain value of one baroreflex system as it operates in openloop conditions. As a result, the normal, dynamic functioning of the arterial and cardiopulmonary baroreflex control of TPR remains to be fully elucidated. To this end, we introduce a signal processing algorithm to identify the TPR baroreflex impulse response (and the dominant time constant of the systemic arterial tree) by analysis of small, beat-to-beat fluctuations in arterial blood pressure, cardiac output, and stroke volume. The algorithm may therefore provide a complete linear dynamic characterization of the TPR baroreflex under normal, closed-loop conditions from totally non-invasive measurement methods (e.g., arterial tonometry and Doppler ultrasound). We also demonstrate the validity of the algorithm with respect to realistic simulated data with known dynamic properties and conscious canine data before and after chronic arterial baroreceptor denervation. With further successful experimental testing, the signal processing algorithm may ultimately be employed to advance the basic understanding of the TPR baroreflex in both humans and animals in health and disease.

## **ACKNOWLEDGMENTS**

Here I would like to thank all the people who have helped me in this work.

First, I am very grateful to my advisor: Dr. Ramakrishna Mukkamala. Dr. Mukkamala helps me finish this very interesting thesis research and always gives me suggestions.

I would also like to thank J. K. Kim, J. Sala-Mercado, R. L. Hammond and D. S. O'Leary from Wayne State University School of Medicine for providing the experimental data used in the evaluation.

I also thank my colleagues Zhenwei Lu and Rafat Inayat Elahi for their advice.

## **TABLE OF CONTENTS**

1.	INTRODUCTION	1
1.1	MOTIVATION	1
1.2	Aims	2
1.3	ORGANIZATION	3
2.	BACKGROUND	4
2.1	BAROREFLEX PHYSIOLOGY	4
2.2	PREVIOUS METHODS FOR MEASURING THE TPR BAROREFLEX	5
3.	SIGNAL PROCESSING ALGORITHM	9
3.1	ESTIMATION OF THE STATIC GAINS OF THE ARTERIAL AND CARDIOPULMO	
TPR	BAROREFLEX SYSTEMS	9
3.2 3.3	ESTIMATION OF THE IMPULSE RESPONSE OF THE ARTERIAL TPR BAROREFL ESTIMATION OF THE IMPULSE RESPONSE OF THE CARDIOPULMONARY TPR	
BAR	OREFLEX	19
3.4	IMPLEMENTATION OF THE SIGNAL PROCESSING ALGORITHM	
4.	EXPERIMENTS AND RESULTS	24
4.1	SIMULATED DATA	24
	4.1.1 Data generation objective	
	4.1.2 Results	27
4.2	Experimental data	29
	4.2.1 Experimental methods	29
	4.2.2 Results	30
5.	CONCLUSIONS AND FUTURE WORK	33
5.1	Conclusions	33
5.2	FUTURE WORK	
RIRI	IOCD A DHV	25

## **LIST OF FIGURES**

Figure 1: Block diagram defining the total peripherial resistance(TPR) baroreflex system to be analyzed
Figure 2: Diagram indicating how arterial blood pressure (ABP) would change over time in response to a step change in cardiac output (CO)
Figure 3: Block diagram indicating step 1 of signal processing algorithm
Figure 4: Block diagram indicating step 2 of signal processing algorithm
Figure 5: A first order RC circuit to represent the systemic arterial tree at low frequencies
Figure 6: Estimation of the RC time constant of the systemic arterial tree
Figure 7: Block diagram summarizing a previously developed human cardiovascular simulator
Figure 8: Simulated and human radial ABP waveforms
Figure 9: Power spectra of heart rate (HR) from the simulated and human experimental data
Figure 10: Actual and estimated arterial TPR baroreflex impulse responses
Figure 11: Sample power spectra before and after chronic arterial baroreceptor denervation from a single dog
Figure 12: Group average arterial and cardiopulmonary TPR baroreflex gain values before and after chronic arterial baroreceptor denervation in seven conscious dogs 32

## **LIST OF TABLES**

Table 1: Conventional methods for measuring the TPR baroreflex	8
Table 2: Actual and estimated G <sub>C</sub> and τ values	28
Table 3: Segments chosen to analyze in conscious dog data	30
Table 4: Group average hemodynamic values of conscious canine data	31

## 1. Introduction

#### 1.1 Motivation

The total peripheral resistance (TPR) baroreflex is one of the most important factors to regulate short-term arterial blood pressure (ABP) on a time scale of seconds to minutes and thus is critical to maintain arterial pressure in response to changing demands on the cardiovascular system.

The traditional techniques used to characterize the TPR baroreflex system involve perturbing the blood pressure with an external stimulus as the input signal, measuring the TPR response as the output signal, and then plotting the stimulus-response curve whose slope indicates the system gain. The external stimuli that have been employed may be broadly classified as selective or non-selective. Selective stimuli only excite one baroreflex system while the non-selective stimuli excite both arterial and cardiopulmonary baroreflex systems simultaneously.

However, these traditional techniques have limitations. The selective stimuli methods open the feedback loop between the baroreflex and circulation and thereby preclude the study during normal physiologic conditions. In contrast, non-selective stimuli methods preserve normal closed-loop conditions, but the unique contribution of each baroreflex system cannot be distinguished from a simple stimulus-response curve. Multiple regression analysis (MRA) [McCullagh et al, 1989] can distinguish the individual gain values of arterial and cardiopulmonary TPR baroreflex systems. However, it requires a sophisticated experimental preparation in which both heart rate (HR) and blood volume are perturbed. As a result, its applications are limited. In addition, the traditional

techniques only provide a static characterization of the TPR baroreflex without explaining the dynamic properties. Thus, a practical technique is needed to characterize the normal, dynamic functioning of the arterial and cardiopulmonary TPR baroreflex systems.

#### 1.2 Aims

To this end, we previously developed a signal processing algorithm to identify the static gains of the arterial TPR baroreflex ( $G_A$ ) and cardiopulmonary TPR baroreflex ( $G_C$ ) by mathematical analysis of the small beat-to-beat fluctuations in ABP, cardiac output (CO), and stroke volume (SV). In this thesis, we aim to extend the signal processing algorithm so as to identify the impulse response characterizing the TPR baroreflex. The extended technique may therefore provide a complete linear dynamic characterization of the TPR baroreflex under normal, closed-loop conditions without application of an external stimulus and from totally non-invasive measurement methods (e.g., Finger-cuff photoplethysmography [Imholz et al, 1998] and Doppler ultrasound [Eriken et al, 1990]). The technique specifically identifies the impulse responses relating the fluctuations in CO to ABP and the fluctuations in SV to ABP and then represents the identified impulse responses with physiologic models so as to estimate the arterial TPR baroreflex impulse response,  $G_C$ , as well as the dominant time constant ( $\tau$ ) of the systemic arterial tree (i.e., the product of TPR and the lumped arterial compliance (AC)).

In this thesis, we also aim to evaluate the technique with respect to both simulated and experimental data. First, we applied the technique to the realistic beat-to-beat variability generated by a cardiovascular simulator whose actual dynamic properties are precisely

determined. Then, we applied the technique to the spontaneous beat-to-beat variability measured from seven conscious dogs before and after chronic arterial baroreceptor denervation.

## 1.3 Organization

This thesis is organized as follows. Chapter 2 provides an overview of the TPR baroreflex systems and the conventional measurement methods. Chapter 3 discusses the signal processing algorithm we developed and its implementation. Chapter 4 describes the simulated and experimental evaluation studies and results. Chapter 5 summarizes the works carried out in this thesis and suggests future directions of study.

## 2. Background

## 2.1 Baroreflex Physiology

The arterial and cardiopulmonary baroreflex systems contribute to the regulation of blood pressures over short time scales of seconds to minutes. The maintenance of blood pressure is vital to the proper functioning of organs such as the brain, heart, and others. Thus, understanding the functioning of these baroreflex systems is very important.

The baroreflex systems operate through negative feedback control of the circulation in which the sensed variables are blood pressures and the controlled variables are circulatory parameters such as HR, TPR, and ventricular contractility (VC). The arterial baroreflex senses ABP via baroreceptors that lie in the wall of the bifurcation region of the carotid arteries in the neck and also in the arch of the aorta in the thorax. The arterial baroreflex system responds to an increase in pressure at its receptors by, for example, decreasing HR, TPR, and VC so as to maintain ABP. The cardiopulmonary baroreceptors reside mostly in the cardiac chambers but also in the walls of the pulmonary artery [Bishop et al, 1983] and are very responsive to changes in central venous pressure (CVP) [Desai et al, 1997; Raymundo et al, 1989]. The cardiopulmonary baroreflex responds to an increase in pressure at its receptors by decreasing TPR [Mancia et al, 1983; Raymundo et al, 1989]. An increase in CVP also leads to an increase in HR in dogs [Bainbridge, 1915], but an opposite change may occur in humans [Desai et al, 1997]. The cardiopulmonary baroreflex is more complicated and is less understood compared to the arterial baroreflex.

The control of HR by the arterial baroreflex is the most extensively studied baroreflex mechanism due to the relative ease of measuring HR and ABP. Previous researchers have studied the HR baroreflex in diabetes mellitus (e.g., [Mukkamala et al, 1999]), heart failure (e.g., [Thames et al, 1993]), and hypertension [Moreira et al, 1992]. However, the HR baroreflex may not be the most important regulator of ABP. Guyton showed that venous return is nearly saturated at normal right atrial pressures due to the collapse of the large veins entering the thorax and thus, ABP can only be enhanced by about 15-20% by increasing only HR (see Figure 4 in [Guyton et al, 1957]). In contrast, all TPR changes are directly transmitted to ABP via Ohmic effects so that the TPR baroreflex may be a more important short-time regulator of ABP.

## 2.2 Previous Methods for Measuring the TPR

#### **Baroreflex**

Among the previous studies of the TPR baroreflex, most employed an external stimulus and followed three steps for characterizing this feedback mechanism: 1) perturb the baroreceptors with an external stimulus; 2) measure the steady-state TPR response; and 3) plot the stimulus-response curve whose slope indicates the system gain. The external stimuli that have been employed may be broadly classified as selective or non-selective. Selective stimuli such as carotid sinus pressure control [Olivier et al, 1993; Schmidt et al, 1971] and lower body negative pressure [Johnson et al, 1974; Zoller et al, 1972] only excite one set of baroreceptors and thus only the system response corresponding to this specific baroreflex system may be determined. However, the selective stimuli approach opens the feedback loop between the baroreflex and

circulation and thereby precludes its study during normal physiologic conditions. In addition, the tenet that only one set of baroreceptors has been perturbed may not always be valid.

The non-selective stimuli such as upright tilting [Waters et al, 2002] excite both arterial and cardiopulmonary baroreflex systems simultaneously. The advantage of the non-selective stimulus approach is that it preserves normal closed-loop conditions. However, the relative contributions of the arterial and cardiopulmonary baroreceptors to the total system response cannot be distinguished without a more sophisticated analysis.

Raymundo et al introduced their approach to measure the TPR baroreflex [Raymundo et al, 1989, which improved upon previous efforts. The central idea of their technique was to perturb all of the baroreceptors by changing the ventricular pacing rate and blood volume which are both non-selective stimuli. Then, they employed the MRA approach to distinguish the contributions of the arterial and cardiopulmonary baroreflex. To be specific, these investigators developed a conscious canine model utilizing the ventricular pacing (50-160 bpm after atrioventricular (AV) block) and blood volume perturbations (±10%) to vary mean CVP and mean ABP independently of each other. That is, changes in the blood volume cause mean CVP and mean ABP to vary in the same direction, while changes in the ventricular pacing rate cause the two pressures to vary in the opposite direction (e.g., [Barcroft et al, 1944; Fisher et al, 1984; Raymundo et al, 1989]). Thus, by combining these two perturbations, a data set was created in which ABP and CVP were orthogonal. With this orthogonal data set, the contribution of the resulting changes in mean CVP and mean ABP to mean TPR (as determined with an aortic flow probe CO measurement) was accurately assessed by MRA in which the two pressures were treated as the independent variables and mean TPR was considered as the dependent variable. The coefficient associated with mean ABP (G<sub>A</sub>) indicated the steady-state TPR change that would occur if the arterial baroreflex was stimulated by a unity step increase in ABP when CVP remained constant, while the coefficient associated with mean CVP (G<sub>C</sub>) indicated the steady-state TPR change that would occur if the cardiopulmonary baroreflex was stimulated by a unity step increase in CVP when ABP remained constant.

Raymundo et al evaluated their technique in five animals during baseline conditions and also under conditions of chronic arterial baroreceptor denervation and then vagal block. Under baseline conditions, both arterial and cardiopulmonary baroreflex systems contributed significantly to TPR control. After arterial baroreceptor denervation, the magnitude of G<sub>A</sub> was reduced essentially to zero, while the magnitude of G<sub>C</sub> increased nearly three-fold probably to compensate for the diminished arterial baroreflex. Subsequent vagal block reduced the magnitude of G<sub>C</sub> to zero as well (i.e., all TPR responses were eliminated). Thus, in their conscious canine model, the sympathetic afferent nerves contributed negligibly to TPR control. Additionally, these investigators extended the MRA to include nonlinear terms (e.g., mean ABP\*CVP as an independent variable whose associated coefficient represents the gain value of the nonlinear TPR baroreflex interaction) but found no statistical evidence of nonlinear baroreflex effects or interactions for each of the three experimental conditions. This particular finding indicates that nonlinear TPR baroreflex behaviors may be insignificant under each investigated condition and over the physiologic range imposed by the ventricular pacing rate and blood volume perturbations. However, the finding does not necessarily preclude nonlinear or more complex behaviors under a different set of physiologic conditions.

While the technique of Raymundo et al provides an effective means to quantify each TPR baroreflex, it requires a sophisticated experimental preparation to change the ventricular pacing rate and blood volume. It is very time-consuming too. Moreover, because of its invasive nature, the technique is essentially limited to animal studies and has not been subsequently employed for further examination of the TPR baroreflex.

Based on what we have discussed above, we summarize the conventional methods to measure the TPR baroreflex and their limitations in Table 1.

Table 1. Conventional methods for measuring the TPR baroreflex

EXISTING TPR BAROREFLEX MEASUREMENT TECHNIQUE	DISAVDANTAGE OF THE TECHNIQUE WITH RESPECT TO THE PROPOSED SIGNAL PROCESSING ALGORITHM
carotid sinus pressure/nerve stimulation	<ol> <li>instrumentation needed to excite carotid sinus baroreceptors</li> <li>TPR baroreflex feedback loop is opened</li> <li>cardiopulmonary baroreceptors may also be stimulated</li> <li>only GA may be determined</li> </ol>
lower body negative pressure (< 20 mmHg)	<ol> <li>lower body negative pressure equipment needed</li> <li>invasive CVP required</li> <li>TPR baroreflex feedback loop is disturbed</li> <li>arterial baroreceptors may also be stimulated</li> <li>only GC may be determined</li> </ol>
upright tilting	<ol> <li>cannot distinguish changes in GA from changes in GC</li> <li>cannot determine changes in GA and GC due to postural changes</li> </ol>
MRA [Raymundo et al, 1989]	ventricular pacing electrodes and atrioventricular block needed     hemorrhage and volume infusions needed     invasive CVP required

Thus, the integrated, dynamic functioning of the TPR baroreflex remains to be fully explained. To this end, a practical technique is needed to measure these dynamics during normal, closed-loop conditions.

## 3. Signal Processing Algorithm

Mukkamala et al previously developed a signal processing algorithm to quantify the static gains (integral of the impulse response) of the arterial TPR baroreflex ( $G_A$ ) and the cardiopulmonary TPR baroreflex ( $G_C$ ) [Mukkamala et al, 2002]. Here, we extend this algorithm to identify the impulse response characterizing the TPR baroreflex by analyzing the naturally occurring, beat-to-beat fluctuations in CO, SV, and ABP, which can be measured non-invasively in humans using, for example, Doppler ultrasound and arterial tonometry. The algorithm thus characterizes the dynamics of the TPR barorflex under normal closed-loop conditions and requires non-invasive measurements.

System identification is one of the key concepts employed in this signal processing algorithm. System identification is a useful engineering approach to build models characterizing the unknown system from measured input and output data. Compared to the power spectral analysis, which only characterizes the system output response, system identification characterizes the system itself, and thus distinguishes changes in actual system functioning from changes in the system input [Ljung, 1987]. Employed in physiologic systems, system identification can estimate the dynamic system properties (input-output transfer relationship) of the physiologic mechanisms.

# 3.1 Estimation of the Static Gains of the Arterial and Cardiopulmonary TPR Baroreflex Systems

The block diagram in Figure 1 is based on the work of Raymundo et al and specifies the arterial and cardiopulmonary TPR baroreflex systems that we seek to characterize. As

shown in Figure 1 and discussed in Chapter 2, the arterial TPR baroreflex couples ABP fluctuations to TPR fluctuations, and the cardiopulmonary TPR baroreflex couples central venous transmural pressure (CVTP) (which is the difference between CVP and intrathoracic pressure (ITP)) fluctuations to TPR fluctuations. (Because CVP is relatively small, CVTP is a more appropriate index of the sensing pressure of the cardiopulmonary baroreflex.) The block diagram also includes an unmeasured perturbing noise source N<sub>TPR</sub>, which reflects the residual variability in TPR that is not accounted for by the baroreflex mechanisms. Such variability may be due to, for example, the autoregulation of local vascular beds and the release of endothelium-derived relaxing factors [Guyton et al, 1996]. However, we note that N<sub>TPR</sub> may be small with respect to the total TPR fluctuations, as Raymundo et al observed no significant changes in TPR despite variations in ABP, CVP, and CO after arterial baroreceptor denervation and vagal block. The block diagram in Figure 1 also assumes that only linear TPR baroreflex dynamics are present, as Raymundo et al suggested that nonlinear TPR baroreflex behaviors may be insignificant under the investigated condition and over the physiologic range imposed by the ventricular pacing rate and blood volume perturbations.

In principle, one would obtain beat-to-beat measurements of ABP, CVTP, and TPR in order to identify the impulse responses characterizing the arterial TPR baroreflex and cardiopulmonary TPR baroreflex and the power spectrum of N<sub>TPR</sub> based on Figure 1. However, in practice, techniques for directly measuring beat-to-beat fluctuations in TPR are not available. Furthermore, invasive procedures are required to measure CVTP. All these facts indicate that this direct identification algorithm needs to be modified to be more practical.

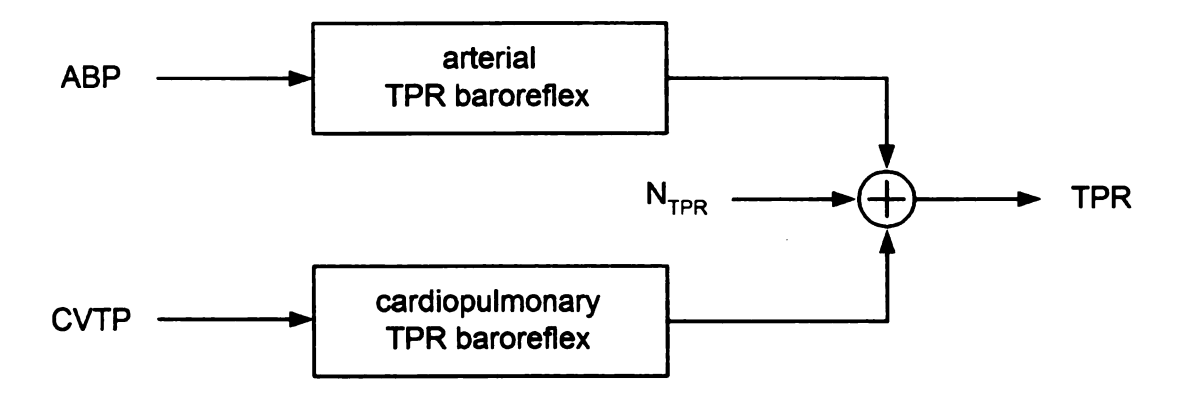


Figure 1. Block diagram defining the total peripheral resistance (TPR) baroreflex system to be analyzed

The measurement of CVTP is very invasive, so we make the assumption that the fluctuations in SV, which can be obtained by dividing CO by HR, are adequate surrogates for the fluctuations in CVTP. In general, changes in left ventricular (LV) SV are caused by changes in LV preload (left atrial (transmural) pressure; LAP), LV afterload (ABP), and VC. However, Suga and Sagawa showed that spontaneous fluctuations in VC are very small at rest [Sagawa et al, 1977]. By accordingly regarding the contribution of resting VC changes to SV changes to be relatively small, we are now able to argue that steady-state SV changes are determined solely by CVTP changes. The pulmonary circulation is a low-pressure circuit with an average pulmonary artery pressure (PAP) of normally 10-15 mmHg. Moreover, PAP is insensitive to CO and LAP over a wide range due to recruitment and distension [Cournand, 1956]. Since the right ventricular (RV) endsystolic elastance is about one mmHg/ml [Dell'Italia et al, 1988], even moderate changes in PAP (RV afterload) would have only a small effect on RV SV. Thus, in steady-state, RV SV is usually determined by only RV preload (CVTP). Since LV SV must equal RV SV on average, steady-state SV changes are therefore determined by only CVTP changes. Although the beat-to-beat LV SV changes are not determined by just CVTP changes, our assumption is specifically that the present CVTP fluctuation is determined by a future LV SV fluctuation as well as present and past LV SV fluctuations. Note that, by inversion, this assumption may be interpreted as the present LV SV fluctuation is determined by the past CVTP fluctuations. Thus, all of these CVTP fluctuations may at least partly account for LV preload and afterload variability.

A straight forward method to estimate the TPR fluctuations is to compute the ratio of average ABP to average CO over intervals in which TPR changes little and net flow through the large compliant arteries is small. It is possible to choose such intervals because the dominant time constant of the systemic arteries (~2 s [Sato et al, 1974]) is smaller than the time constant governing changes in TPR (~ 10 s [Berger et al, 1989]). And we take SV fluctuations as the surrogate for CVTP fluctuations as discussed above, so we can directly estimate the arterial and cardiopulmonary TPR baroreflex through Figure 1. However, a previous study [Mukkamala et al, 2003] has shown that this direct estimation of TPR fluctuations imposes a nonphysiological relationship between the direct identification inputs and the direct identification output as follows

$$\frac{\Delta TPR}{\overline{TPR}}(t) \approx \frac{\Delta ABP}{\overline{ABP}}(t) - \frac{\Delta SV}{\overline{SV}}(t) - \frac{\Delta HR}{\overline{HR}}(t) \tag{1}$$

where each fractional quantity here reflects relative fluctuations with respect to mean values. This relationship erroneously suggests that the arterial TPR baroreflex and SV—ABP step responses are unit step functions scaled by 1 and -1, respectively.

To account for the unmeasured TPR fluctuations, our signal processing algorithm therefore employs the concept that the dynamic relationship between the fluctuations in ABP and CO reflects the fluctuations in TPR caused by the baroreflex. Suppose that the cardiopulmonary TPR baroreflex is inactive (i.e.,  $G_C = 0$ ) and there is a step change in CO, as shown in the top panel of Figure 2. If the arterial TPR baroreflex is also inactive

(i.e.,  $G_A$  =0), then, by Ohm's law, the steady-state fractional change in ABP would equal the fractional change in CO (i.e.,  $\frac{\Delta ABP}{\overline{ABP}} = \frac{\Delta CO}{\overline{CO}}$ ). In contrast, if the arterial TPR baroreflex is active (i.e.,  $G_A$  <0), then the steady-state fractional change in ABP would be less than that of CO due to the accompanying drop in TPR (i.e.  $\frac{\Delta ABP}{\overline{ABP}} < \frac{\Delta CO}{\overline{CO}}$ ). The difference between these two situations indicates the functioning of the arterial TPR baroreflex. That gives us the conceptual basis to characterize the arterial TPR baroreflex by identifying the relationship between fluctuations in CO and ABP.

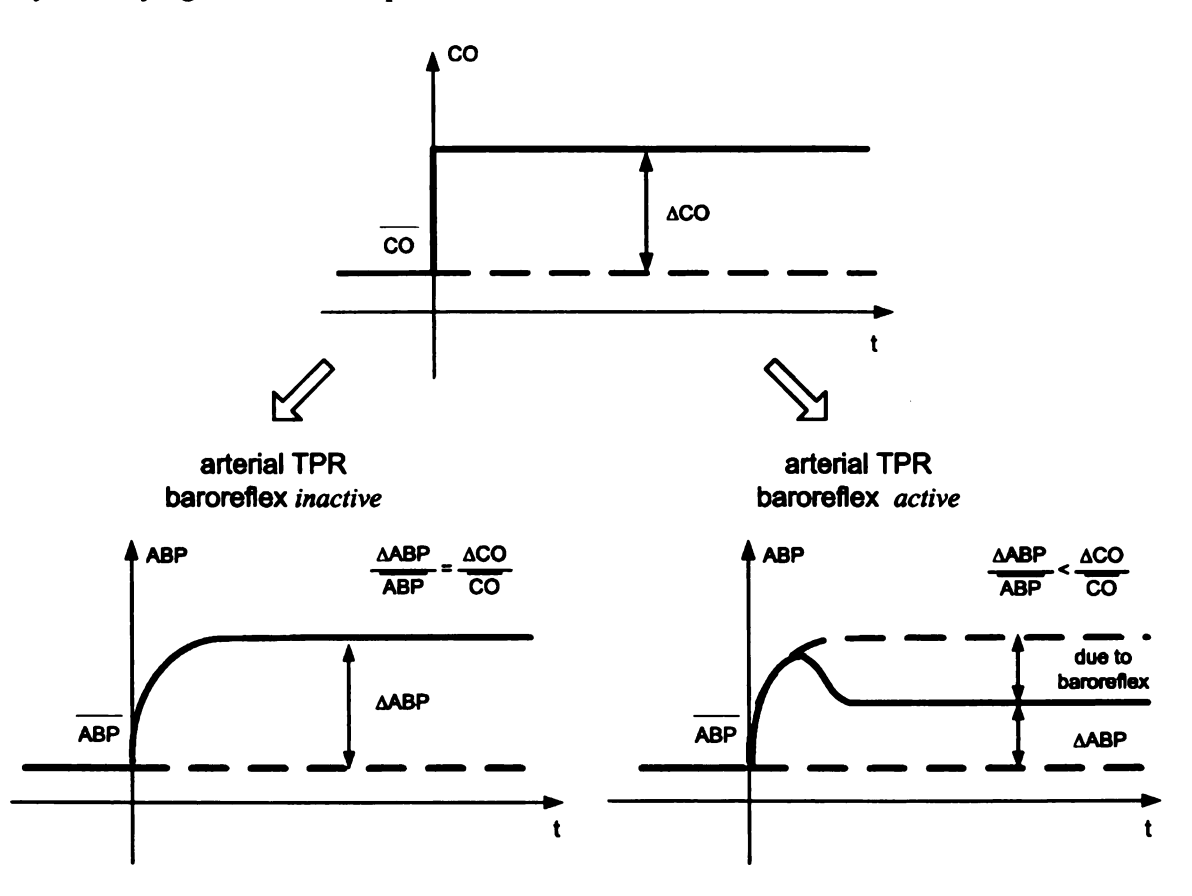


Figure 2. Diagram indicating how arterial blood pressure (ABP) would change over time (t) in response to a step change in cardiac output (CO), if both the arterial TPR baroreflex and cardiopulmonary TPR baroreflex were inactive (lower left panel) and if only the arterial TPR baroreflex were active (lower right panel)

Finally, the block diagram indicating our signal processing algorithm is shown in Figure 3 (step 1 of signal processing algorithm), which accounts for the unmeasured TPR and CVTP fluctuations as discussed above. Here we assume that the measured fluctuations in CO, SV, and ABP are sufficiently small and stationary so that the autonomic coupling mechanisms may be represented by linear time-invariant (LTI) transfer functions. N<sub>ABP</sub> reflects the residual variability in ABP fluctuations that is not accounted for by the CO and SV fluctuations. We employed the system identification approach to estimate the impulse response of from CO to ABP and from SV to ABP. Figure 4 (step 2 of signal processing algorithm) indicates the physiologic models that couple CO to ABP and from SV to ABP. We calculated the static gains of arterial and cardiopulmonary TPR baroreflex, i.e., G<sub>A</sub> and G<sub>C</sub>, based on these models.

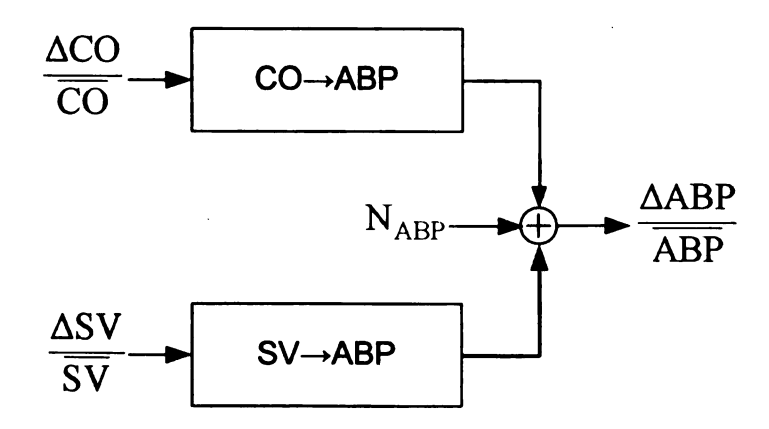


Figure 3. Block diagram indicating step 1 of signal processing algorithm

The mechanism coupling CO to ABP, which is indicated by CO→ABP, includes the dynamic properties of the arterial TPR baroreflex as well as the systemic arterial tree according to Figure 4 (a). This feedback hierarchy shows that an increase in CO will initially cause ABP to increase via the systemic arterial tree. This will excite the arterial TPR baroreflex/systemic arterial tree arc to decrease TPR to maintain ABP.

The static gain of the arterial TPR baroreflex  $(G_A)$  can be computed from the static gain of CO $\rightarrow$ ABP, because the static gain of the systemic arterial tree is identical to one due to the normalization of all signals with their respective mean values. Also due to this normalization, the static gains of CO $\rightarrow$ ABP and arterial TPR baroreflex will be unitless.  $G_A$  indicates the steady-state percent change in TPR (with respect to its mean value) that would occur, if the arterial TPR baroreflex was simulated by an X percent step change in ABP (with respect to its mean value) through the product of X and  $G_A$ .

The mechanism coupling SV to ABP, which is indicated by SV—ABP, includes the dynamic properties of the arterial TPR baroreflex and cardiopulmonary TPR baroreflex as well as the inverse heart-lung unit and systemic arterial tree according to Figure 4 (b). The heart-lung unit is defined to precisely couple CVTP fluctuations to SV fluctuations (according to the above assumption) [Herndon et al, 1969]. So the inverse heart-lung unit precisely couples SV fluctuations to CVTP fluctuations. The feedback hierarchy in Figure 4 (b) shows that an increase in SV will initially cause CVTP to increase via the inverse heart-lung unit. This CVTP increase will excite the cardiopulmonary TPR baroreflex to decrease TPR. This decrease in TPR will then excite the arterial TPR baroreflex/systemic arterial tree arc to increase TPR to maintain ABP.

The static gain of the cardiopulmonary TPR baroreflex can be computed from the static gains of arterial TPR baroreflex and SV $\rightarrow$ ABP because the static gains of the systemic arterial tree and inverse heart-lung unit are identical to one due to the normalization of the signals with their respective mean values. Similarly, the static gains of SV $\rightarrow$ ABP and cardiopulmonary TPR baroreflex are also unitless due to the normalization.  $G_C$  indicates the steady-state percentage change in TPR (with respect to its

mean value) that would occur, if the cardiopulmonary TPR baroreflex was simulated by an X percent step change in CVTP (with respect to its mean value) through the product of X and  $G_{\mathbb{C}}$ .

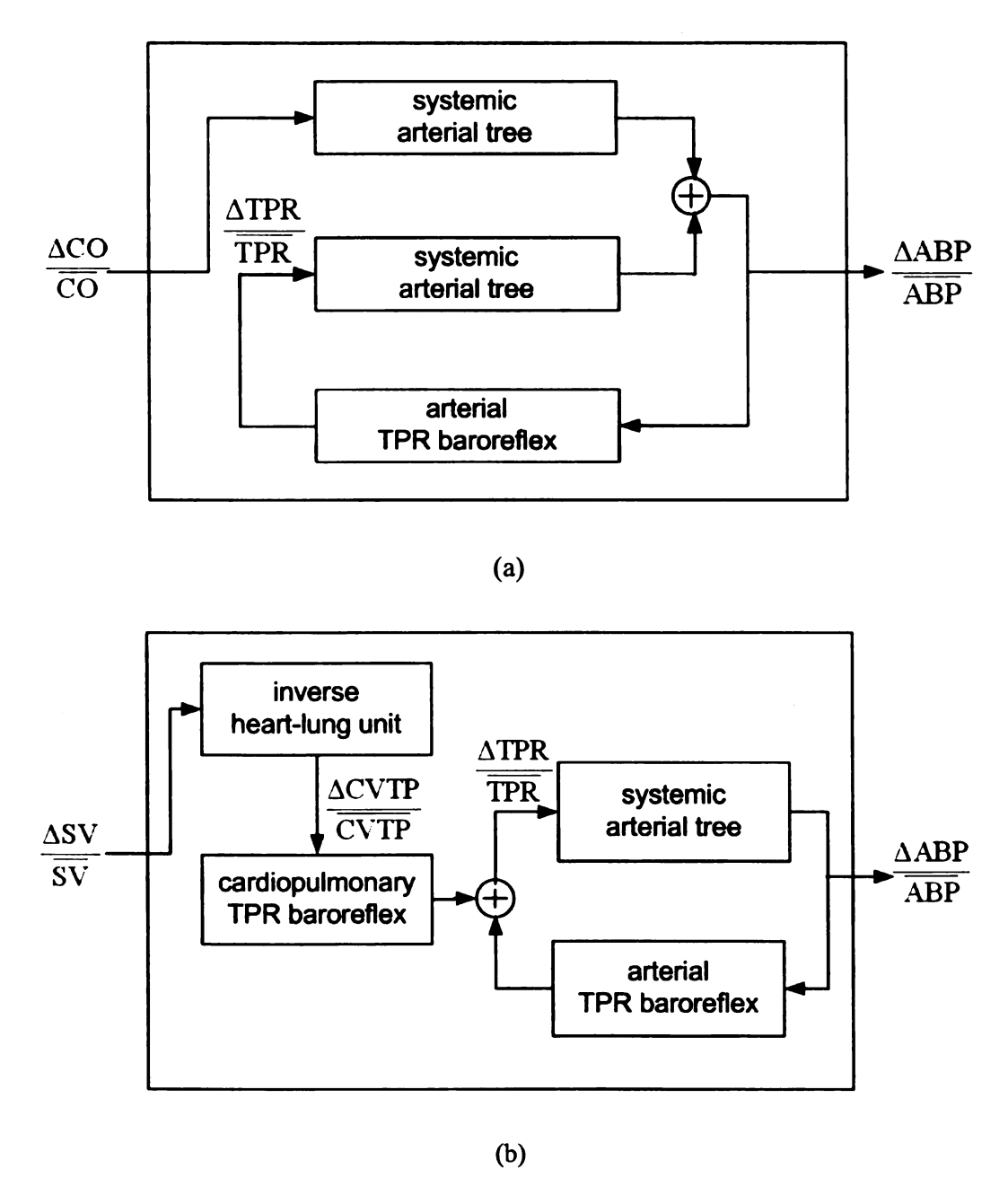


Figure 4. Block diagrams indicating step 2 of signal processing algorithm. The two block diagrams are physiologic models of the internal dynamics of (a) CO $\rightarrow$ ABP and (b) SV $\rightarrow$ ABP in Figure 3

## 3.2 Estimation of the Impulse Response of the Arterial

#### **TPR Baroreflex**

To extend this signal processing algorithm to estimate the TPR baroreflex impulse response, we reconsider the physiologic model of Figure 4 (a). It implies that the impulse response of the arterial TPR baroreflex can be computed through the feedback hierarchy, if both the impulse response of CO→ABP and the impulse response of the systemic arterial tree are known. The impulse response of CO→ABP can be obtained by system identification as described in Section 3.1. So we extended the algorithm to estimate the impulse response of the systemic arterial tree also from the observed beat-to-beat fluctuations in CO and ABP.

We know from physiology that: 1) the distributed systemic arterial tree may be regarded as a lumped system as shown in Figure 5, which is characterized by a single time constant  $\tau$  ( $\tau$  is equal to the product of TPR and AC) for the slow, beat-to-beat fluctuations considered here [Noordergraaf et al, 1978] and 2) TPR baroreflex dynamics are delayed with respect to, and slower than, systemic arterial tree dynamics [Mukkamala et al, 2003]. The extended algorithm therefore aims to estimate the value of  $\tau$  and then the impulse response of the systemic arterial tree which is given by

$$h_{sys}(t) = \frac{1}{\tau} e^{\frac{-t}{\tau}} u(t) \tag{2}$$

where u(t) is the unit step function.

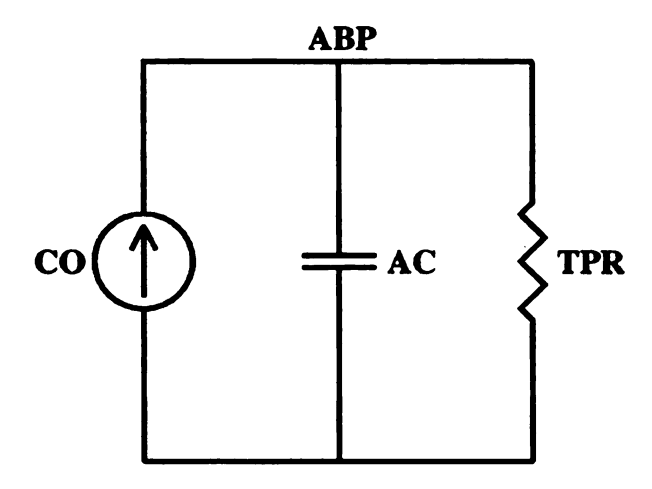


Figure 5. A first order RC circuit to represent the systemic arterial tree at low frequencies

Figure 6 shows the estimation of  $\tau$  by the least square fitting of the systemic arterial tree step response (which is the integral of the impulse response in Equation 1) to the initial upstroke of the CO $\rightarrow$ ABP step response in which the TPR baroreflex has not taken effect (see Figure 2).

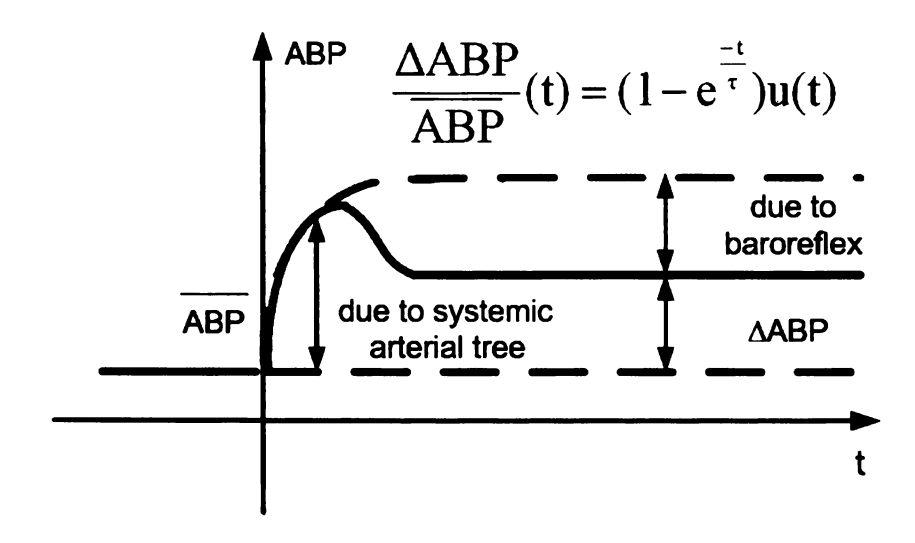


Figure 6. Estimation of the RC time constant of the systemic arterial tree

According to the feedback hierarchy in Figure 4 (a), the impulse response of the arterial TPR baroreflex ( $h_{ATPR}$ ) can be computed from the impulse responses of CO $\rightarrow$ ABP ( $h_{CO\rightarrow ABP}$ ) and the systemic arterial tree ( $h_{sys}$ ).

## 3.3 Estimation of the Impulse Response of the

### **Cardiopulmonary TPR Baroreflex**

According to the feedback hierarchy in Figure 4 (b), the impulse response of the cardiopulmonary TPR baroreflex can be calculated, if given the impulse responses of SV-ABP, systemic arterial tree, arterial TPR baroreflex, and inverse heart-lung unit. However, we do not propose a method to estimate the impulse response of the inverse heart-lung unit. So, the direct estimation of the cardiopulmonary TPR baroreflex impulse response through Figure 4 (b) is not possible. However, we know that both arterial and cardiopulmonary TPR baroreflex systems are governed by the α-sympathetic nervous system. So, it might be reasonable to assume that they have the same dynamics. That is, the impulse response of the cardiopulmonary TPR baroreflex may be identical to that of the arterial TPR baroreflex in shape but scaled in magnitude. Based on the static gain values of arterial and cardiopulmonary TPR baroreflex (GA and GC) and the impulse response of arterial TPR baroreflex we already obtained, we could therefore calculate the impulse response of the cardiopulmonary TPR baroreflex by scaling the impulse response of the arterial TPR baroreflex by  $\frac{G_C}{G_c}$ .

## 3.4 Implementation of the Signal Processing Algorithm

The block diagram shown in Figure 3 can be mathematically represented by an autoregression moving average (ARMA) equation as follows

$$\frac{\Delta ABP}{\overline{ABP}}(t) = \sum_{i=1}^{m} a_i \frac{\Delta ABP}{\overline{ABP}}(t-i) + \sum_{i=0}^{n} b_i \frac{\Delta CO}{\overline{CO}}(t-i) + \sum_{i=0}^{p} c_i \frac{\Delta SV}{\overline{SV}}(t-i) + W_{ABP}(t)$$
(3)

 $\frac{\Delta CO}{\overline{CO}}$ ,  $\frac{\Delta SV}{\overline{SV}}$  and  $\frac{\Delta ABP}{\overline{ABP}}$  in Equation 3 represent the measured beat-to-beat

fluctuations in these signals. The three sets of unknown parameters  $\{a_i, b_i, c_i\}$  define the impulse responses of CO $\rightarrow$ ABP and SV $\rightarrow$ ABP. The terms m, n, p limit the number of parameters (model order), and  $W_{ABP}$  is the unmeasured residual error. This residual error together with the set of parameters  $\{a_i\}$  fully defines the power spectrum of  $N_{ABP}$ .

Because the original signals we have are the continuous recordings of ABP, CO and SV. So we first averaged these signals by replacing their values for current cardiac cycles by the average values of the three previous and three subsequent cardiac cycles. We then resampled the averaged signals at 0.5 Hz with an anti-aliasing filter whose impulse response is unit-area boxcar of four seconds' duration. Finally, we subtracted the means from these signals and divided them by the means to obtain the deviations of the signals from their mean values. Through the above steps, we normalized the signals by their mean values and obtained the fluctuations of these signals, which are used as the inputs and outputs of Equation 3.

Starting from using a maximal model order 3 (i.e., m=n=p=3) and employing a previously developed system identification algorithm [Perrott et al, 1996] which intelligently reduces the model order, we estimate the three sets of parameters  $\{a_i, b_i, c_i\}$ .

Then, according to the physiologic models in Figure 4, the static gains of the arterial and cardiopulmonary TPR baroreflex, i.e.,  $G_A$  and  $G_C$ , are computed from the parameter sets  $\{a_i, b_i, c_i\}$  as follows

$$G_A = \left(\sum_{i=0}^n b_i + \sum_{i=1}^m a_i - 1\right) / \sum_{i=0}^n b_i$$
 (4)

$$G_C = \sum_{i=0}^{p} c_i / \sum_{i=0}^{n} b_i . {5}$$

In principle, this algorithm will be effective provided that spontaneous HR variability is present. If HR variability is deemed to be insignificant with respect to CO variability (e.g., <5%), then only the CO $\rightarrow$ ABP impulse response may be reliably identified (via a single-input ARMA equation). However, in this case, the model of this physiologic system becomes the sum of the block diagrams in Figure 4 with a static gain (G<sub>L</sub>) given as follows

$$G_L = \frac{1 + G_C}{1 - G_A}. (6)$$

Thus, when HR variability is virtually absent, the algorithm estimates  $G_L$  and therefore cannot distinguish between the functioning of the arterial TPR baroreflex and cardiopulmonary TPR baroreflex. However, note that  $G_L$  provides a quantitative measure of the lumped functioning of the two TPR baroreflex mechanisms.

By transferring all the impulse responses to the z-domain, we obtain the z-transform of the impulse response of the arterial TPR baroreflex, denoted as  $H_{ATPR}(z)$ , as follows

$$H_{ATPR}(z) = \frac{H_{CO \to ABP}(z) - H_{sys}(z)}{H_{CO \to ABP}(z)H_{sys}(z)}$$
(7)

where  $H_{ATPR}(z)$ ,  $H_{CO\to ABP}(z)$  and  $H_{sys}(z)$  are the z-transform of  $h_{ATPR}$ ,  $h_{CO\to ABP}$  and  $h_{sys}$ , respectively.

Due to noise, we noticed that some zeros of the estimated  $H_{CO\to ABP}(z)$  reside outside of the unit circle. These zeros will cause system instability in  $H_{ATPR}(z)$  [Oppenheim et al, 1997] because all the zeros of  $H_{CO\to ABP}(z)$  becomes the poles of  $H_{ATPR}(z)$  according to Equation 7.

To solve this instability problem, we tracked these zeros outside of the unit circle in  $H_{CO \to ABP}(z)$  and found that they were corresponding to the high frequency components in CO $\to$ ABP impulse response. So we employed a low pass filter to remove these high frequency components and thus remove all the zeros outside of the unit circle to make the system invertible. The cut-off frequency of this low pass filter is chosen to be 0.1 Hz [Berger et al, 1989]. We employed this low pass filter on the CO $\to$ ABP impulse response obtained from the system identification, and then compensated the phase delay caused by this filter to realize a zero-phase filtering.

To obtain the impulse response of the systemic arterial tree, we integrated the estimated impulse response of CO $\rightarrow$ ABP before the low pass filtering to obtain the step response of CO $\rightarrow$ ABP (solid line in Figure 6). According to the analysis in Section 3.2, the initial upstroke of the first three seconds in this step response is only governed by the systemic arterial tree since the slower TPR baroreflex has not taken effect yet. This initial upstroke corresponds to the first two samples in the step response of CO $\rightarrow$ ABP since our sampling frequency is 0.5 Hz. We fit the systemic arterial tree step response to these two samples through the minimum mean square error (MMSE) method to find the best estimation of the time constant  $\tau$ . Then the impulse response of the systemic arterial tree is generated through Equation 1.

We also low pass filtered the impulse response of the systemic arterial tree through the same zero phase filter employed on the impulse response of CO→ABP.

Finally, the impulse response of the arterial TPR baroreflex  $(h_{ATPR})$  is calculated according to Equation 7 and we also low pass filtered  $h_{ATPR}$  by the same zero phase filter employed before.

By employing the same filter on  $h_{CO \to ABP}$ ,  $h_{sys}$  and  $h_{ATPR}$ , we cancel the effects of these low pass filters ideally at the end and make Equation 7 hold exactly. To be specific, suppose the z-transform of this low pass filter is G(z), then  $H_{CO \to ABP}(z)$  becomes  $H_{CO \to ABP}(z)G(z)$  and  $H_{sys}(z)$  becomes  $H_{sys}(z)G(z)$  after filtering. Substitute  $H_{CO \to ABP}(z)$  by  $H_{CO \to ABP}(z)G(z)$  and  $H_{sys}(z)G(z)$  and  $H_{sys}(z)$  by  $H_{sys}(z)G(z)$  in Equation 7 and the output  $H^{'}_{ATPR}(z)$  becomes

$$H'_{ATPR}(z) = \frac{H_{CO \to ABP}(z)G(z) - H_{sys}(z)G(z)}{(H_{CO \to ABP}(z)G(z))(H_{sys}(z)G(z))} = \frac{H_{CO \to ABP}(z) - H_{sys}(z)}{H_{CO \to ABP}(z)H_{sys}(Z)G(z)}$$
(8)

As described before, we also employed the same low pass filter on  $H'_{ATPR}(z)$ . So the output of this filter, which is the z-transform of our estimated  $h_{ATPR}$ , becomes

$$H_{ATPR}(z) = H'_{ATPR}(z)G(z) = \frac{H_{CO \to ABP}(z) - H_{sys}(z)}{H_{CO \to ABP}(z)H_{sys}(z)}$$
(9)

which is exactly the same as the one without low pass filtering. So we canceled the impact of the low pass filter and exactly followed the algorithm that we developed above.

## 4. Experiments and Results

#### 4.1 Simulated Data

#### 4.1.1 Data Generation Objective

We generated six-minute intervals of simulated data with beat-to-beat variability from a previously developed computational simulator of human cardiovascular system [Mukkamala et al, 2003]. We applied our signal processing algorithm to these data to estimate the static gains of the arterial and cardiopulmonary TPR baroreflex, the impulse response of the arterial TPR baroreflex, and the time constant of the systemic arterial tree. Independently, we applied an arbitrary narrow unit-area input to the appropriate point in the cardiovascular simulator to establish the gold standard impulse responses of the arterial and cardiopulmonary TPR baroreflex.

The block diagram shown in Figure 7 illustrates the major components of this cardiovascular simulator. It includes three major components: a pulsatile heart and circulation, a short-term regulatory system, and resting physiological perturbations. The circulatory system consists of contracting left and right ventricles, systemic arteries and veins, and pulmonary arteries and veins. The systemic arteries are specifically modeled as a third-order system accounting for viscous, compliant, and inertial effects. The regulatory system comprises arterial and cardiopulmonary baroreflex control of HR, TPR, systemic venous unstressed volume (SVUV), and VC as well as a direct neural coupling between respiration and HR. Each baroreflex effector system is specifically modeled as a static non-linearity to account for saturation followed by linear dynamics.

The resting perturbations include respiratory activity, stochastic disturbances to TPR and SVUV, and 1/f HR fluctuations.

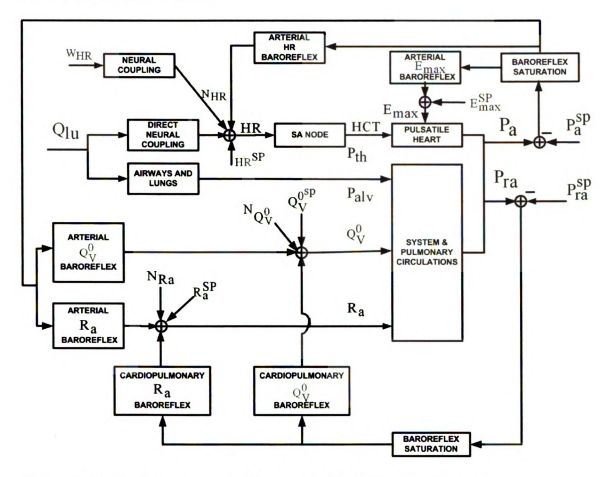


Figure 7. Block diagram summarizing a previously developed human cardiovascular simulator [Mukkamala et al, 2003]

As shown in Figure 8, the simulated ABP waveform resembles human radial ABP waveform, which demonstrates the cardiovascular simulator can generate realistic signal waveforms. Figure 9 illustrates that the power spectrum of HR from the simulated data resembles that of the human data, which demonstrates the cardiovascular simulator can generate realistic beat-to-beat variability of signals.

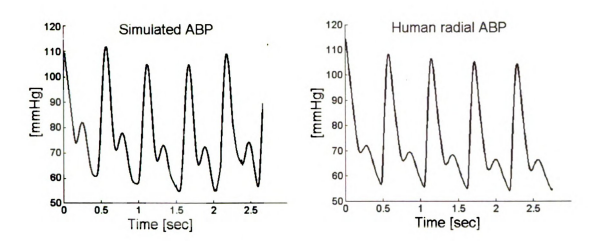


Figure 8. Simulated and human radial ABP waveforms

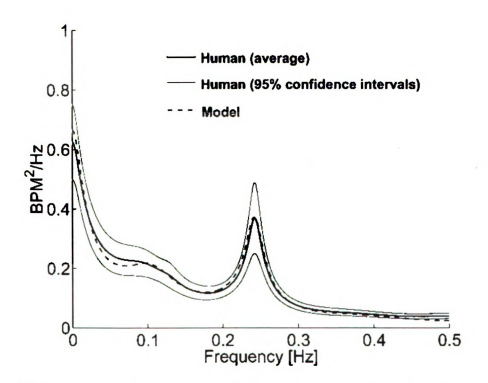


Figure 9. Power spectra of heart rate (HR) from the simulated and human experimental data  $\,$ 

Our specific goal was to determine if the technique can accurately estimate, and detect changes in the impulse response of the arterial TPR baroreflex, the static gain value of the cardiopulmonary TPR baroreflex,  $G_C$ , and the dominant time constant  $\tau$  of the systemic arterial tree. In order to achieve this goal, we conducted a series of simulations under different sets of parameter values. For each set of parameter values, we repeated the simulation 50 times to determine the mean and 95% confidence intervals of the estimates. To evaluate the estimates, we established the corresponding actual  $\tau$  value by taking the product of the total AC and the mean TPR and the actual arterial and cardiopulmonary TPR baroreflex impulse responses by isolating these systems from the simulator, applying an impulse input to each system, and measuring the TPR response. The areas of these impulse responses were then computed so as to establish the actual  $G_A$  and  $G_C$  values.

### 4.1.2 Results

Figure 10 illustrates the actual and estimated arterial TPR baroreflex impulse responses for different simulator  $G_A$  values. Table 2 shows the actual and estimated  $G_C$  for different simulator  $G_C$  values as well as the actual and estimated  $\tau$  for different simulator total AC values.

These results show that the technique is able to accurately estimate, and detect changes in, the arterial TPR baroreflex impulse response and  $\tau$ . Because SV fluctuations do not perfectly represent CVTP fluctuations, the results also indicate that the technique has consistently underestimated  $G_C$ . However, the algorithm is able to detect changes in the simulator  $G_C$  value.

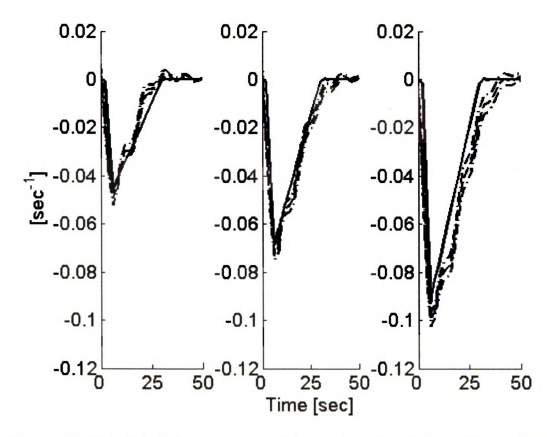


Figure 10. Actual (solid) and estimated (mean (dash)  $\pm$  95% confidence intervals (dash-dot)) arterial TPR baroreflex impulse responses

Table 2. Actual and estimated (mean±95% confidence intervals)  $G_C$  and  $\tau$  values

Gc [unitless]		τ [sec]		
ACTUAL	ESTIMATE	ACTUAL	ESTIMATE	
-0.37	-0.15±0.02	1.06	1.13±0.02	
-0.55	-0.29±0.02	1.56	1.64±0.03	
-0.74	-0.50±0.03	2.08	2.19±0.05	

# 4.2 Experimental Data

## 4.2.1 Experimental methods

We analyzed the experimental data from seven conscious dogs before and after chronic arterial baroreceptor denervation. We applied our signal processing algorithm to these data to specifically identify the arterial and cardiopulmonary TPR baroreflex gain values.

Researchers at the Wayne State University School of Medicine collected the hemodynamic data utilized in our evaluation, and the materials and methods were described in detail in a very recently published study [Kim et al, 2005]. We described here the most basic aspects of the experimentation that were relevant to our evaluation. Seven conscious dogs (20-25 kg) of either gender were studied according to the following protocol. Chronic instrumentation was installed in each dog to measure central ABP, CO, HR, and other hemodynamic variables. After recovery from the surgery, the beat-to-beat hemodynamic data were recorded for about ten minutes while the dog was standing quietly. Then, surgical denervation of the carotid sinus and aortic arch receptors was performed. The completion of the baroreceptor denervation was confirmed by observing the lack of any HR response to an intravenous bolus infusion of phenylephrine, which increased ABP by ~40 mmHg. Finally, approximately two weeks after the completion of the baroreceptor denervation, the beat-to-beat hemodynamic data were again recorded for about ten minutes while the dogs were standing quietly.

We choose the segments shown in Table 3 of the experimental data of each dog visually to include as much "clean data" as possible before and after chronic arterial baroreceptor denervation. "End" indicates the end of the individual data set.

Table 3. Segments chosen to analyze in conscious dog data

DOG NAME	SEGMENTS CHOSEN			
DOG NAME	BEFORE	AFTER		
ВО	70:end	50:end		
СНІ	61:274	1:170		
CR	70:end	1:410		
HAS	1:end	40:end		
LU	85:end	300:end		
МО	60:end	1:end		
ROK	60:280	1:end		

#### 4.2.2 Results

Table 4 illustrates that the group mean hemodynamic values did not change in response to chronic arterial baroreceptor denervation. The "blindness" of the mean hemodynamic values to baroreflex functioning is consistent with the notion that the baroreflex is not important in long-term blood pressure regulation. The standard deviation of ABP significantly increased from 2.9 mmHg to 10.2 mmHg after the chronic arterial baroreceptor denervation. The power spectra in Figure 11 show that the fluctuations of the hemodynamic variables about their mean values were altered by chronic arterial baroreceptor denervation, especially the fluctuations in ABP increased significantly. This is because the chronic arterial baroreceptor denervation reduced the ability to maintain blood pressure. However, it is still impossible to "see" the effects of the denervation specifically on TPR baroreflex functioning.

Table 4. Group average hemodynamic values (mean±95% confidence intervals) of conscious canine data

HEMO- DYNAMIC VARIABILITY	CHRONIC ARTERIAL BARORECEPTOR DENERVATION				
	BEFORE		AFTER		
	MEAN	STDEV	MEAN	STDEV	
ABP [MMHG]	105.9±12.3	2.9±0.7	117.2±14.0	10.2±4.5	
CO [ML/S]	80.6±9.9	6.2±3.0	79.7±13.5	5.3±1.8	
SV [ML]	46.1±6.0	2.4±2.9	37.7±4.9	2.0±0.6	
HR [BPS]	1.8±0.2	0.2±0.1	2.1±0.3	0.1±0.1	

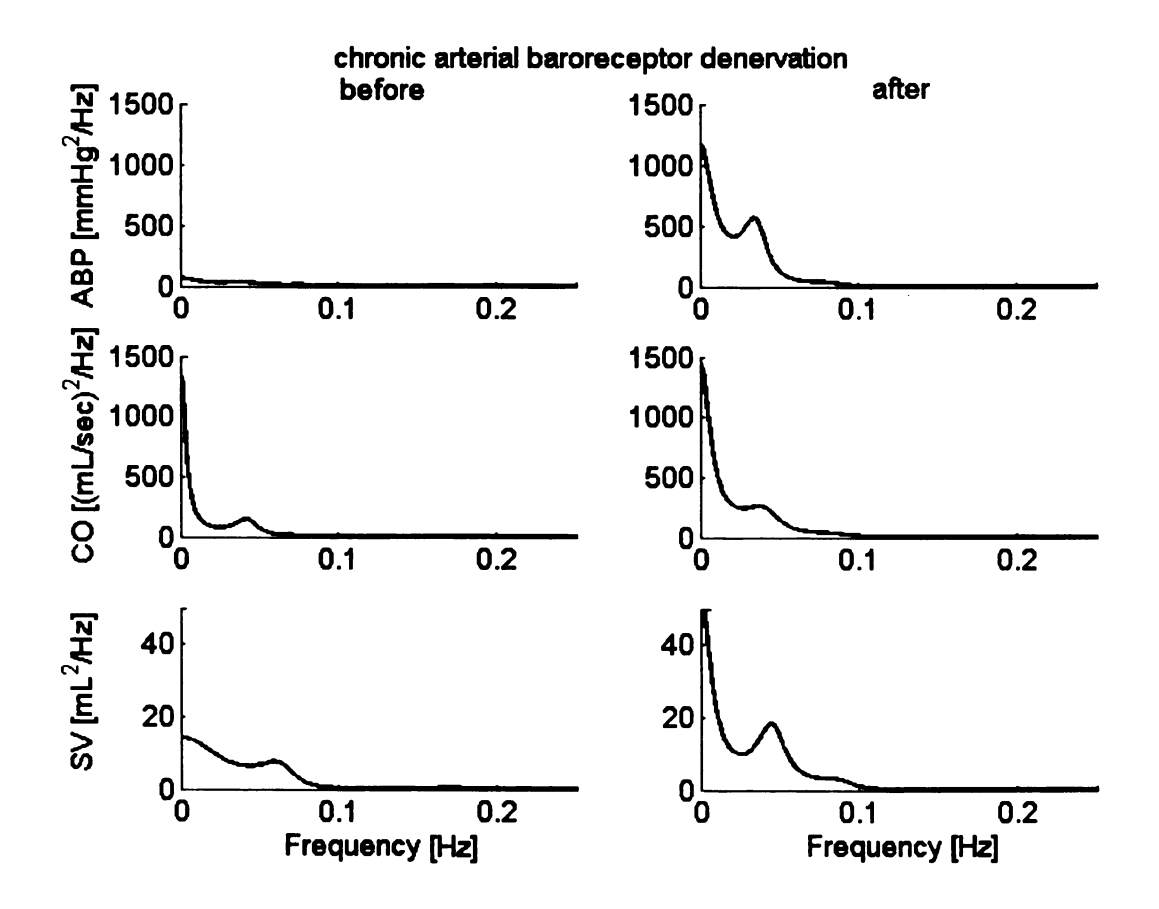


Figure 11. Sample power spectra before and after chronic arterial baroreceptor denervation from a single dog

Figure 12 illustrates the group average estimates of  $G_A$  and  $G_C$  (mean±stdev) before and after chronic arterial baroreceptor denervation by employing our algorithm on these canine data. It indicates that our algorithm predicted that chronic arterial baroreceptor denervation caused the magnitude of  $G_A$  to reduce to nearly zero (i.e., arterial TPR baroreflex functioning was lost) and the magnitude of  $G_C$  to more than double (i.e., cardiopulmonary TPR baroreflex functioning was enhanced) to compensate. Both changes were statistically significant. These results are consistent with the very invasive MRA method for quantifying the TPR baroreflex gain values [Raymundo et al, 1989]. The estimated  $G_A$  and  $G_C$  values in Figure 12 are, on average, roughly 2-3 times as large as the values reported by Raymundo et al. These differences may be due to different postures and signal normalization schemes as well as inter-subject variability.

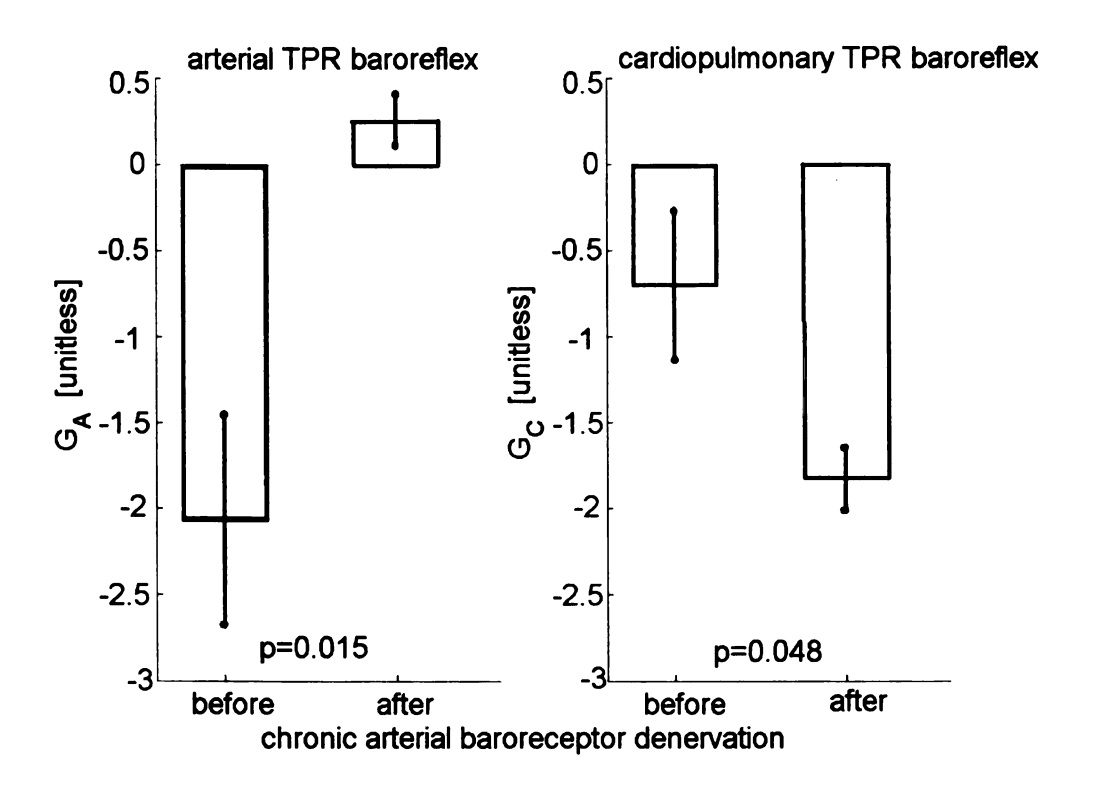


Figure 12. Group average arterial and cardiopulmonary TPR baroreflex gain values before and after chronic arterial baroreceptor denervation in seven conscious dogs

# 5. Conclusions and Future Work

## 5.1 Conclusions

In this thesis, we discussed the theoretical fundamental and the implementation of a signal processing algorithm, which can be employed on the continuous measurements of CO, ABP and SV to identify the dynamic functioning of the TPR baroreflex. It is a noninvasive technology and keeps the normal, closed-loop conditions of the TPR baroreflex systems. We also covered the evaluation of this algorithm by both simulated data generated from a cardiovascular simulator and experimental data collected from seven conscious dogs.

The main contributions of this research are as follows:

- 1) It developed a signal processing algorithm to estimate the impulse response of the arterial TPR baroreflex from the continuous measurements of CO, ABP, and SV.
- 2) It validated the signal processing algorithm by simulated data and experimental data.

## 5.2 Future Work

The impulse response of the TPR baroreflex of the conscious dogs remains undetermined in this thesis. And we do not have the corresponding gold standard dynamics against which we can compare our results with.

In the future, we will study the conscious dogs to compare the TPR gain values determined by our algorithm with the ones obtained by applying MRA to ABP, CO and CVTP measured during a set of adjustments to the ventricular pacing rate and blood

volume [Raymundo et al, 1989]. We will also evaluate the ability of our algorithm in determining the subtle changes in TPR baroreflex functioning. Those changes, which may be excited by the usage of medicine, will be a practical test conditions for our algorithm.

With further successful experimental testing, the technique presented in this thesis may ultimately be employed to advance the basic understanding of the TPR baroreflex in both humans and animals in health and disease.

# **BIBLIOGRAPHY**

Akselrod, S., D. Gordon, F. A. Ubel, D. C. Shannon, A. C. Barger, R. J. Cohen. Power spectrum analysis of heart rate fluctuation: a quantitative probe of beat-to-beat cardiovascular control. Science, 213:220-222, 1981.

Akselrod, S., D. Gordon, J. B. Madwed, N. C. Snidman, D. C. Shannon, R. J. Cohen. Hemodynamic regulation: investigation by spectral analysis. Am. J. Physiol., 249(18):H867-H875, 1985

Aljuri, N., R. Marini, R. J. Cohen. Test of dynamic closed-loop baroreflex and autoregulatory control of total peripheral resistance in the intact and conscious sheep. Am. J. Physiol., Jul 1 [Epub ahead of print], 2004.

Appel, M. L., R. D. Berger, J. P. Saul, J. M. Smith, R. J. Cohen. Beat to beat variability in cardiovascular variables: noise or music? JACC, 14(5):1139-1148, 1989.

Bainbridge, F. A. The influence of venous filling upon the rate of the heart. J. Physiol. Lond., 50:65-84, 1915.

Barcroft, H. J., J. McMichael, O. G. Edholm, E. P. Sharpey-Schafer. Posthaemorrhagic fainting. Study by cardiac output and forearm flow. Lancet, 1:489-491, 1944.

Berger, R. D., J. P. Saul J P, R. J. Cohen. Assessment of autonomic response by broadband respiration. IEEE Trans. Biomed. Eng., 36:1061-1065, 1989a.

Berne, R. M., M. N. Levy. Cardiovascular Physiology. The C. V. Mosby Company, St. Louis, MO, 1986.

Bertinieri, G., M. Di Rienzo, A. Cavallazzi, A. U. Ferrari, A. Pedotti, F. Mancia G. Evaluation of baroreceptor reflex by blood pressure monitoring in unanesthetized cats. Am. J. Physiol., 254:H377-383, 1988.

Bishop, V. S., A. Malliani, P. Thoren. Cardiac mechanoreceptors. In: Handbook of Physiology. The Cardiovascular System. Peripheral Circulation and Organ Blood Flow. Bethesda, MD: Am. Physiol. Soc., sect. 2, vol. III, pt. 2, chapt. 15, 497-555, 1983.

Bourgeois, M. J., B. K. Gilbert, D. E. Donald, E. H. Wood. Characteristics of aortic diastolic pressure decay with application to the continuous monitoring of changes in peripheral resistance. Circ. Res., 35:56-66, 1974.

Charkoudian, N., E. A. Martin, F. A. Dinenno, J. H. Eisenach, N. M. Dietz, M. J. Joyner. Influence of increased central venous pressure on baroreflex control of sympathetic activity in humans. Am. J. Physiol., 287(4):H1658-H1662, 2004.

Chon, K. H., T. J. Mullen, R. J. Cohen. A dual-input nonlinear system analysis of autonomic modulation of heart rate. IEEE Trans. Biomed. Eng., 43:530-544, 1996.

Cournand, A. F. http://nobelprize.org/medicine/laureates/1956/cournand-lecture.html, 1956.

Dampney, R. A. L., M. G. Taylor, E. M. McLachlan. Reflex effects of stimulation of carotid sinus and aortic baroreceptors on hindlimb vascular resistance in dogs. Circ. Res., 29(2):119-127, 1971.

Dell'Italia, L. J., R. A. Walsh. Application of a time varying elastance model to right ventricular performance in man. Cardiovasc. Res., 22(12):864-874, 1988.

Desai, T. H., J. C. Collins, M. Snell, R. Mosqueda-Garcia. Modeling arterial and cardiopulmonary baroreflex control of heart rate. Am. J. Physiol., 272(41):H2343-H2352, 1997.

Eriksen, M., L. Walloe. Improved method for cardiac output determination in man using ultrasound Doppler technique. Med. Biol. Eng. Comput., 28:555-560, 1990.

Ferguson, D. W., F. M. Abboud, A. L. Mark. Selective impairment of baroreflex-mediated vasoconstrictor responses in patients with ventricular dysfunction. Circulation, 69:451-460, 1984.

Fisher, S. J. A. M. Scher, C. R. Wyss. Longer term responses of atrial rate and peripheral resistance to changes in ventricular pacing rate in awake dogs with atrioventricular block. Circ. Res., 54:196-203, 1984.

Freeman, R., J. P. Saul, M. S. Roberts, R. D. Berger, C. Broadbridge, R. J. Cohen. Spectral analysis of heart rate in diabetic autonomic neuropathy. A comparison with standard tests of autonomic function. Arch. Neurol., 48(2):185-190, 1991.

Guyton, A. C., J. E. Hall. Textbook of Medical Physiology. W. B. Saunders Company, Philadelphia, 1996.

Guyton, A. C., A. W. Lindsey, B. Abernathy, T. Richardson. Venous return at various right atrial pressure and the normal venous return curve. Am. J. Physiol., 189(3):609-615, 1957.

Hales, S. Haemastaticks. In: Statistical Essays. London: Innings and Manby, vol. II, 1733.

Hallock, P., J. C. Benson. Studies on the elastic properties of human isolated aorta. Am. J. Physiol., 16:595-602, 1937.

Hamlin, R. L., T. Nakayama. Comparison of some pharmacokinetic parameters of 5 angiotensin-converting enzyme inhibitors in normal beagles. J. Vet. Intern. Med., 12(2):93-95, 1998.

Heldt, T., E. B. Shim, R. D. Kamm, R. G. Mark. Computational modeling of cardiovascular response to orthostatic stress. J. Appl. Physiol., 92(3):1239-1254, 2002.

Herndon, C. W., K. Sagawa. Combined effects of aortic and right atrial pressures on aortic flow. Am. J. Physiol., 217(1):65-72, 1969.

Hirsch, J. A., B. Bishop. Respiratory sinus arrhythmia in humans: how breathing pattern modulates heart rate. Am. J. Physiol., 241:H620-629, 1981.

Imholz, B. P. M., W. Wieling, G. A. van Montfrans, K. H. Wesseling. Fifteen years experience with finger arterial pressure monitoring: Assessment of the technology. Cardiovasc. Res., 38:605-616, 1998.

Jacobsen, T. N., B. J. Morgan, U. Scherrer, S. F. Vissing, R. A. Lange, N. Johnson, W. S. Ring, P. S. Rahko, P. Hanson, R. G. Victor. Relative contributions of cardiopulmonary and sinoaortic baroreflexes in causing sympathetic activation in the human skeletal muscle circulation during orthostatic stress. Circ. Res., 73:367-378, 1993.

James, J. E., B. Daly Mde. Comparison of the reflex vasomotor responses to separate and combined stimulation of the carotid sinus and aortic arch baroreceptors by pulsatile and non-pulsatile pressures in the dog. J. Physiol., 209(2):257-293, 1970.

Johnson, J. M., L. B. Rowell, M. Niederberger, M. M. Eisman. Human splanchnic and forearem vasoconstrictor responses to reductions of right atrial and aortic pressure. Circ. Res., 34:51-524, 1974.

Karunanithi M. K., M. P. Feneley. Single-beat determination of preload recruitable stroke work relationship: derivation and evaluation in conscious dogs. J. Am. Coll. Cardiol., 35(2):502-513, 2000.

Kaufman, E. S., M. S. Bosner, J. T. Bigger, P. K. Stein, R. E. Kleiger, L. M. Rolnitzky, R. C. Steinman, J. L. Fleiss. Effects of digoxin and enalapril on heart period variability and response to head-up tilt in normal subjects. Am. J. Cardiol., 72(1):95-99, 1993.

Kitney, R. I. Entrainment of the human RR interval by thermal stimuli. J. Physiol. Lond., 252:37P-38P, 1975.

Kleiger, R. E., J. P. Miller, J. T. Bigger, A. J. Moss. Decreased heart rate variability and its association with increased mortality after acute myocardial infarction. Am. J. Cardiol., 59:256-262, 1987.

Kim, J. K., Sala-Mercado, J.A., Rodriguez, J., Scislo, T.J., O'Leary, D.S., Arterial baroreflex alters strength and mechanisms of muscle metaboreflex during dynamic exercise. Am. J. Physiol., vol. 288, pp. H1374-H1380, 2005.

Lanfranchi, P. A., V. K. Somers. Arterial baroreflex function and cardiovascular variability: interactions and implications. Am. J. Physiol., 283:R815-R826, 2002.

Leja, F. S., D. E. Euler, P. J. Scanlon. Digoxin and the susceptibility of the canine heart to countershock-induced arrhythmia. Am. J. Cardiol., 55(8):1070-1075, 1985.

Ljung, L. System Identification: Theory for the User. PTR Prentice Hall, Englewood Cliffs, NJ, 1987.

Mancia, G., A. L. Mark. Arterial baroreflexes in humans. In: Handbook of Physiology. The Cardiovascular System. Peripheral Circulation and Organ Blood Flow, Bethesda, MD: Am. Physiol. Soc., sect. 2, vol. III, pt.2, chapt. 20, 755-793, 1983.

McCullagh, P., J. Nelder. Generalized Linear Models. Chapman & Hall, London, 1989.

Moreira, E. D., F. Ida, V. L. Oliveira, E. M. Krieger. Early depression of the baroreceptor sensitivity during onset of hypertension. Hypertension, 19:II198-II201,1992.

Mukkamala, R., R. J. Cohen. A forward model-based validation of cardiovascular system identification. Am J. Physiol., 281:H2714-H2730, 2001.

Mukkamala, R., J. M. Mathias, T. J. Mullen, R. J. Cohen, R. Freeman. System identification of closed-loop cardiovascular control mechanisms: Diabetic autonomic neuropathy. Am. J. Physiol., 276:R905-R912, 1999.

Mukkamala, R., A. T. Reisner, H. M. Hojman, R. G. Mark, R. J. Cohen. Continuous cardiac output monitoring by peripheral blood pressure waveform analysis. Comput. Cardiol., 29:561-564, 2003.

Mukkamala, R., K. Toska, R. J. Cohen. Noninvasive identification of the total peripheral resistance baroreflex. Am. J. Physiol., 284:H947-H959, 2003b.

Mullen, T. J., M. L. Appel, R. Mukkamala, J. M. Mathias, R. J. Cohen. System identification of closed-loop cardiovascular control: Effects of posture and autonomic blockade. Am. J. Physiol., 272:H448-H461, 1997.

Noordergraaf, A. Circulatory System Dynamics. New York: Academic Press, 1978.

O'Leary, D. S., N. F. Rossi, P. C. Churchill. Muscle metaboreflex control of vasopressin and rennin release. Am. J. Physiol., 264(5 Pt 2):H1422-7, 1993.

Olivier, N. B., R. B. Stephenson. Characterization of baroreflex impairment in conscious dogs with pacing-induced heart failure. Am. J. Physiol., 265(34):R1132-R1140, 1993.

Oppenheim, A., Willsky, A., Nawab, S., Signals & systems. Upper Saddle River, N.J.: Prentice Hall, c1997.

Perrott, M. H., R. J. Cohen. An efficient approach to arma modeling of biological systems with multiple inputs and delays. IEEE Trans. Biomed. Eng., 43(1):1-14, 1996.

Raymundo, H., A. M. Scher, D. S. O'Leary, P. D. Sampson. Cardiovascular control by arterial and cardiopulmonary baroreceptors in awake dogs with atrioventricular block. Am. J. Physiol., 257(26):H2048-H2058, 1989.

Sagawa, K., H. Suga, A. A. Shoukas, K. M. Bakalar. End-systolic pressure/volume ratio: A new index of ventricular contractility. Am. J. Cardiol., 40:748-753, 1977.

Sanders, J. S., A. L. Mark, D. W. Ferguson. Importance of aortic baroreflex in regulation of sympathetic responses during hypotension. Evidence from direct sympathetic nerve recordings in humans. Circulation, 79:83-92, 1989.

Sato T, Yamashiro SM, Vega D, Grodins FS. Parameter sensitivity analysis of a network model of systemic circulatory mechanics. Ann Biomed Eng 2: 289-306, 1974.

Schmidt, R. M., M. Kumada, K. Sagawa. Cardiac output and total peripheral resistance in carotid sinus reflex. Am. J. Physiol., 221(2):480-487, 1971.

Siebert, J., P. Drabik, R. Lango, K. Szyndler. Stroke volume variability and heart rate power spectrum in relation to posture changes in healthy subjects. Med. Sci. Monit., 10(2):MT31-37, 2004.

Soderstrom, T., P. Stoica. System Identification. Prentice Hall Inc., Englewood Cliffs, NJ, 1989.

Steiner, C., A. T. W. Kovalik. A simple technique for production of chronic complete heart block in dogs. J. Appl. Physiol., 25:631-632, 1968.

Thames, M. D., T. Kinugawa, M. L. Smith, M. E. Dibner-Dunlap. Abnormalities of baroreflex control in heart failure. J. Am. Coll. Cardiol., 22[Supplement A]:56A-60A, 1993.

Toska, K., M. Eriksen. Application of a time varying elastance model to right ventricular performance in man. J. Physiol., 472:501-512, 1993.

Tripathi, A., G. Mack, E. R. Nadel. Peripheral vascular reflexes elicited during lower body negative pressure. Aviat. Space Environ. Med., 60:1187-1193, 1989.

Victor, R. G., A. L. Mark. Interaction of cardiopulmonary and carotid baroreflex control of vascular resistance in humans. J. Clin. Invest., 76:1592-1598, 1985.

Waters, W. W, M. G. Ziegler, J. V. Meck. Postspaceflight orthostatic hypotension occurs mostly in women and is predicted by low vascular resistance. J. Appl. Physiol., 92(2):586-594, 2002.

Zoller, R. P., A. L. Mark, F. M. Abboud, P. G. Schmid, D. D. Heistad. The role of low pressure baroreceptors in reflex vasoconstrictor responses in man. J. Clin. Invest., 51:2967-2972, 1972.

